Thermofluid analysis of an Axial Flux Permanent Magnet (AFPM) generator

R. Wang,[1] **R.T. Dobson**[2] and **M.J. Kamper**[3]

(First received October 2000; Final version February 2001)

In this article a lumped-parameter heat transfer model and an air flow model of a typical Axial Flux Permanent Magnet (AFPM) machine is presented. The application of the proposed models to an AFPM generator is described in detail. The calculated results are compared with the measurements taken from a prototype AFPM machine. The advantages and disadvantages of the approach are then outlined and conclusions drawn. The developed thermofluid model is shown to perform thermal analyses with reasonable accuracy.

Nomenclature

A	cross-section area of a flow path (m^2)
C_{mo}	moment coefficient
c_p	specific heat at constant pressure (J/kg K)
D	diameter (m)
D_h	hydraulic diameter (m)
D_o	outer diameter of electric machine (m)
F	friction force (N)
G	gap ratio, s/r_o
Gr	Grashof number
h	local heat transfer coefficient (W/m^2 K)
I_{ph}	phase current of the machine (A)
i	enthalpy (J/kg)
k	thermal conductivity (W/m K)
k_i	loss coefficient
k_s	slip factor
M_o	momentum (N · s)
$\dot{m}$	mass flow rate (kg/s)
n	machine rotation speed (r.p.m.)
n_b	number of blades
Nu	Nusselt number
P	power (W)
P_r	Prandtl number
p	pressure (Pa)
$\wp$	wetted perimeter
$\dot{Q}$	heat transfer rate into a system (W)
Q	volumetric flow rate (m^3/s)
R	thermal resistance (K/W)
R or r, r_o	radius, outer radius (m)
Ra	Rayleigh number
Re	Reynolds number
s	axial gap between rotor and stator (m)
T	temperature (°C or K)
U	internal energy (J/kg)
u_1, u_2	inlet, outlet tangential velocity (m/s)
v_1, v_2	inlet, outlet absolute velocity (m/s)
$\dot{W}$	rate of doing work (W)
w_1, w_2	inlet, outlet radial velocity (m/s)

Greek symbols

ρ	density (kg/m^3)
β	coefficient of thermal expansion (K^{-1})
ϵ	emissivity
σ	Stefan-Boltzmann constant (W/m^2 K^4)
ω	angular velocity (rad/s)
μ	dynamic viscosity (kg/m s)
ν	kinematic viscosity (m^2/s)
λ	friction factor
λ_T	turbulent parameter
γ	equivalent sand grain roughness (m)
Δ	finite difference

Subscripts

a	surrounding air
ag	air-gap
amb	ambient
$c, conv$	convection
cs	control surface
Cu	Copper
cv	control volume
$cond$ or d	conduction
e	environment, exit
edy	eddy current
f	friction
h	hydraulic
i	in, inlet, input
l	energy losses
m	magnet
mo	moment
out	output
p	periphery
r	radiation, rotor
T	turbulent
t	total
wf	windage and friction

[1] Department of Electrical Engineering, University of Stellenbosch, Private Bag X1, Matieland, 7602, South Africa

[2] Department of Mechanical Engineering, University of Stellenbosch

[3] Department of Electrical Engineering, University of Stellenbosch

Introduction

The advent of new high energy product permanent magnet (PM) materials has shown great opportunities for novel topologies of electrical machines with advantageous features such as high efficiency and power/weight ratio. The AFPM machine (Figure 1), with slotless winding and axially directed magnetic field crossing the air-gap, has remarkably short axial length and can find applications in power generation, electric vehicle (EV) drives, electric pump and fan drives, and domestic appliances. In view of its disc-type configuration, AFPMs are particularly suitable for the development of compact integrated power generation systems, which can be used in South African rural areas.

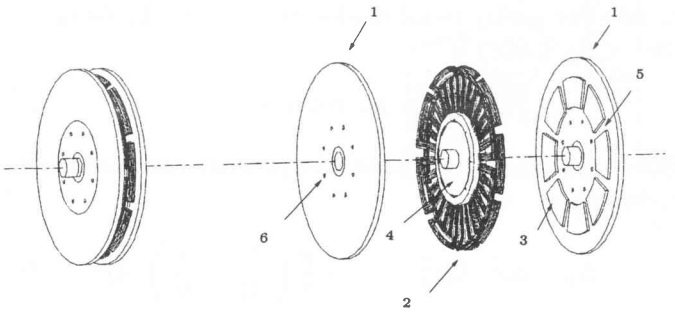

Figure 1 Exploded view of an AFPM machine,
1 - rotor discs, 2 - stator winding, 3 - permanent magnets,
4 - epoxy core, 5 - radial channels, 6 - air-inlet holes

Whereas extensive research has been devoted to thermal studies of conventional electrical machines, AFPM machines have received very little attention.[1] Since AFPM machines possess relatively large air-gap volume and quite often have multi-gaps, the general perception is that AFPM machines have better ventilation capacity than their radial field counterparts.[2,3] However, like conventional machines, AFPM machines are also subject to cooling problems. To ensure a long operational life for the machine, the heat generated must be removed from the machine so that the temperature limitations established for the machine materials such as insulating materials, lubricants and permanent magnets are complied with. Besides, lower operating temperature reduces extra copper losses introduced by the temperature coefficient of the winding resistance. Thus, quantitative studies of the heat dissipation potential of AFPM machines with vastly different topologies are clearly needed.

This paper presents the thermofluid analysis of an AFPM generator. First, the fluid flow model of a prototype AFPM machine is developed, where the relationships between flow rate and rotating speed are obtained. With this information available, a lumped-parameter heat transfer model of the AFPM generator is then derived and used to estimate the operating temperatures in various parts of the machine for different power generating conditions. Experimental tests are also done on the prototype machine and results are compared with the calculated ones.

Objective

The objective of this research was to develop a thermofluid model of a typical AFPM machine based on one dimensional fluid and heat flow. The accuracy and consistency of the derived model are assessed by comparing the calculated flow rate and temperature values of a prototype machine with the measured ones. The causes of discrepancies are discussed and recommendations of improving the model are made.

Fluid flow model

Closely examining the machine structure, shown in Figure 1, reveals that an air stream will be drawn through the air inlet holes into the machine and then forced outwards in the radial channel as the rotor discs rotate. The PMs in fact act as impeller blades. The study of the fluid behavior of the AFPM machine is much like that of a centrifugal fan.

The ideal radial channel

According to the theory of an ideal impeller, a number of assumptions have to be made to establish the one- dimensional flow model of the ideal radial channel:[4,5]

(a) the inlet flow to the channel is radial,

(b) no tangential flow component in the radial channels,

(c) the flow is incompressible and frictionless, and

(d) the velocity variation across the width or depth of the channel is zero.

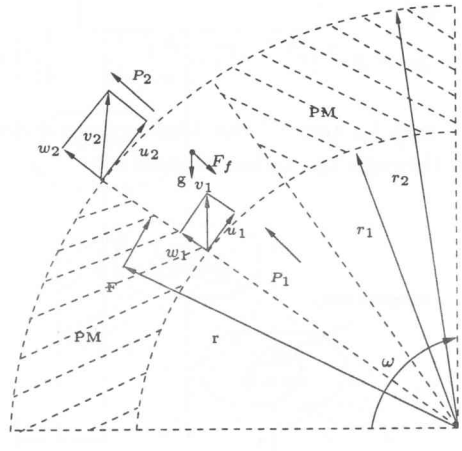

Figure 2 Velocity triangles for a PM channel

Figure 2 shows a radial channel with the velocity triangles drawn at the inlet and the outlet. It can be observed that the pressure at the inlet p_1 and the outlet p_2, and the

friction F_f have no contribution to the sum of the momentum, $\sum M_0$. Ignoring gravity, the general representation of conservation of momentum takes the form:[6]

$$\sum M_0 = \frac{\partial}{\partial t}\left[\int_{cv} (\vec{r} \times \vec{u})\, \rho dV\right] + \int_{cs} (\vec{r} \times \vec{u})\, \rho\, (\vec{w} \cdot \vec{n})\, dA \tag{1}$$

For steady-state one-dimensional air flowing between the entrance and exit of the channel Eqn. 1 may be simplified as:

$$\sum M_0 = T_0 = (\vec{r}_2 \times \vec{u}_2)\, \dot{m}_2 - (\vec{r}_1 \times \vec{u}_1)\, \dot{m}_1 \tag{2}$$

where $\dot{m}_2 = \dot{m}_1 = \rho Q$, and $u = \omega r$. The input shaft power $\dot{W}_i$ is then given by:

$$\dot{W}_i = T_0 \cdot \omega = \rho Q \omega^2 \left(r_2^2 - r_1^2\right) \tag{3}$$

Re-arranging the above equation gives:

$$\frac{\dot{W}_i}{Q} = \rho \omega^2 \left(r_2^2 - r_1^2\right) \tag{4}$$

Based on the principle of conservation of energy, the input shaft power may be given as:

$$\dot{W}_i = \dot{m}\left(\frac{p_2 - p_1}{\rho} + \frac{w_2^2 - w_1^2}{2} + z_2 - z_1 + U_2 - U_1\right) \tag{5}$$

Ignoring potential $(z_2 - z_1)$ and the internal energy (friction), Eqn. 5 may be written in the same units as Eqn. 4 as:

$$\frac{\dot{W}_i}{Q} = (p_2 - p_1) + \rho \frac{w_2^2 - w_1^2}{2} \tag{6}$$

Equating Eqn. 4 and Eqn. 6 and noting that $w_1 = Q/A_1$ and $w_2 = Q/A_2$ (A_1 and A_2 are cross-section area of the inlet and outlet channel, respectively), the pressure difference Δp between the entrance and exit of the radial channel (shown in Figure 2) may be expressed as:

$$\Delta p = p_2 - p_1 = \rho \omega^2 \left(r_2^2 - r_1^2\right) - \frac{\rho}{2}\left(\frac{1}{A_2^2} - \frac{1}{A_1^2}\right) Q^2 \tag{7}$$

Eqn. 7 may be termed the *ideal* equation describing the air flow through the radial channel.

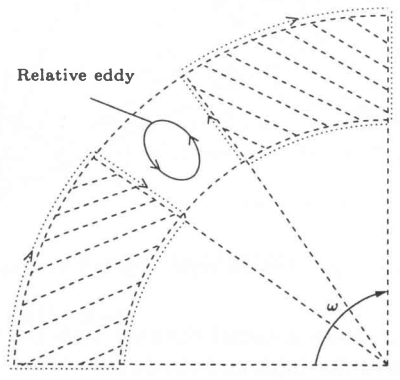

Figure 3 The relative eddy in the PM channel

The actual radial channel

The actual characteristics of a hydraulic machine differ from the ideal case due to two reasons: the uneven spatial distribution of velocities in the blade passages, and the leakage and recirculation of flow and hydraulic losses such as friction and shock losses. These are completely different issues[4] and will be dealt with separately in the following two sections as *slip* and *shock, leakage and friction.*

Slip

As a result of the unbalanced velocity distribution on the leading and trailing edges of a PM channel and rotation effects,[5] there exists, due to Stodola, a *relative eddy*[5,7] within the blade passage shown in Figure 3. This results in the reduction of the tangential velocity components and is called *slip*, which is usually accounted for using a *slip factor*. For purely radial blades, the *Stanitz* slip factor k_s ($80° < \beta_2 < 90°$) is

$$k_s = 1 - 0.63\pi/n_b \tag{8}$$

When applying a slip factor, the pressure relations (Eqn. 8) becomes

$$\Delta_p = \rho \omega^2 \left(k_s r_2^2 - r_1^2\right) + \frac{\rho}{2}\left(\frac{1}{A_1^2} - \frac{1}{A_2^2}\right) \cdot Q^2 \tag{9}$$

Shock, leakage and friction

Energy losses due to friction, separation of the boundary layer (shock loss) and leakage should also be considered.

As illustrated in Figure 4, if the total volumetric flow rate through the PM channel is Q_t, the pressure difference between the PM exit and the entrance will cause a *leakage* or recirculation of a volume of fluid Q_l, thus reducing the flow rate at outlet to $Q = Q_t - Q_l$. The Q_l is a function of mass flow rate and discharge and leakage path resistances. The leakage flow reaches its maximum when the main outlet flow is shut.

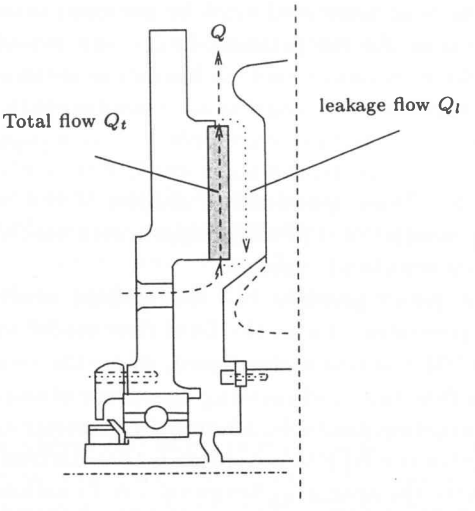

Figure 4 Leakage flow in an AFPM machine (not to scale)

These losses can be accounted for by introducing a pressure loss term Δp_l in Eqn. 9 as follows[5]

$$\Delta p = \rho\omega^2 \left(k_s r_2^2 - r_1^2\right) + \frac{\rho}{2}\left(\frac{1}{A_1^2} - \frac{1}{A_2^2}\right) \cdot Q^2 - \Delta p_l \quad (10)$$

System losses

As the air passes through the AFPM machine, the system pressure loss due to friction must be accounted for. The sum of these losses is given by:

$$\Delta p_f = \frac{\rho Q^2}{2} \sum_{i=1}^{n} \frac{k_i}{A_i^2} \quad (11)$$

There are a number of sections through which the air flows in the AFPM machine (see Figure 5):

1. Entry to the rotor air inlet holes
2. Passage through rotation short pipe
3. Bending of air from pipe to annulus (90°)
4. Round bend air passage (90°)
5. Contraction of air in tapering passage
6. Bending of air through the 90° elbow
7. Entry to permanent magnet channels
8. Expansion of air through tapering enlargement
9. Abrupt expansion of air on the exit of the channel
10. Expansion as the air leaves the opening of the parallel rotor discs

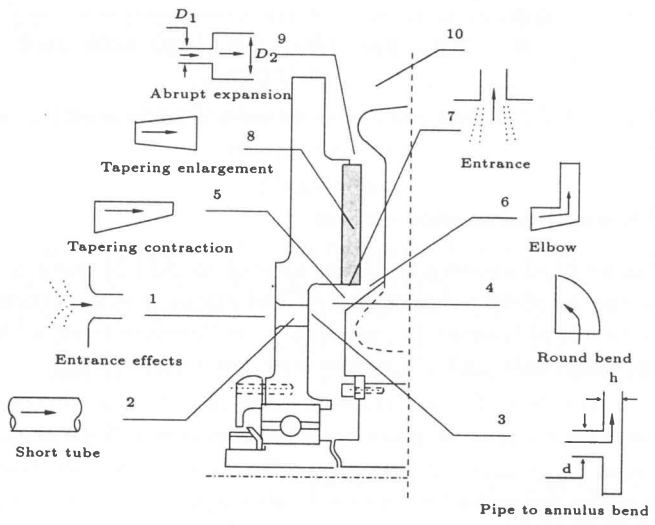

Figure 5 System losses of an AFPM machine

The loss coefficients associated with each section are readily available in the literature.[7,8,9] Where the section is not circular, use has been made of the hydraulic diameter to characterize the cross-section. The hydraulic diameter is defined as $D_h = 4A/\wp$ where A is the cross-sectional area of the flow path and $\wp$ is the wetted perimeter.

The loss coefficient for a pipe is given by $\lambda L/d$ where λ is a friction factor obtained as a function of Re and surface roughness from a *Moody diagram.*[10] To facilitate numeric calculations, the Moody diagram may be represented by:[8]

$$\begin{cases} \lambda &= 8\left[\left(\frac{8}{\mathrm{Re}}\right)^{12} + \frac{1}{(A+B)^{3/2}}\right]^{1/12} \\ A &= \left[2.457 \cdot \ln\left\{\frac{1}{(7/\mathrm{Re})^{0.9} + 0.27\gamma/D}\right\}\right]^{16} \\ B &= \left[\frac{37530}{\mathrm{Re}}\right]^{16} \end{cases} \quad (12)$$

where $\mathrm{Re} = \frac{\rho D_h Q}{\mu A}$.

Characteristics

It is now possible to relate the theoretical prediction obtained from the ideal flow model to the actual characteristic by accounting for the various losses discussed above.

Since the AFPM machine (Figure 1) has two identical coaxial rotating discs operating on the same stator, it may be treated as two identical fans in parallel. The characteristic curve presented in this section represents only half of the AFPM machine. The characteristic curve of the whole machine may be obtained by adding flow rate at the same pressure.

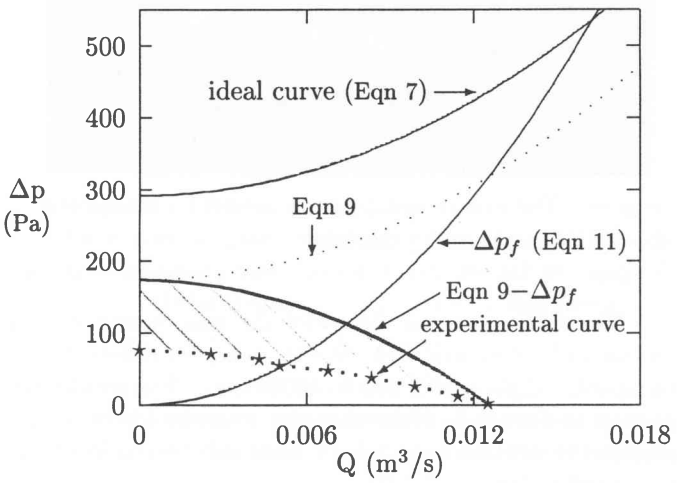

Figure 6 Losses and characteristics curves at 1200 r.p.m

Assuming that the AFPM machine operates at a constant speed of 1 200 r.p.m., the ideal developed pressure characteristic for a radial channel is a function described by Eqn. 7 as shown in Figure 6. After introducing the slip factor, the resultant curve is shown in dotted line as Eqn. 9. It was not possible to obtain a suitable correlation in the literature[11] for the pressure loss due to shock and leakage as was the case for the slip. The calculated characteristic curve without considering shock and leakage losses (Eqn. $9 - \Delta p_f$) shown in Figure 6 is significantly higher than the experimental one. The shaded area in Figure 6 represents the shock and leakage losses. It can be seen that at low flow rates the shock and leakage losses are greater but tend

to zero at the maximum flow rate. The calculated maximum flow rate point corresponds with the experimental curve. Although it could be a coincidence, it may be assumed at this stage that the influence of shock and leakage losses at the maximum flow rate is insignificant.

Flow and pressure measurements

In order to check the validity of the fluid flow model, experimental tests were performed. The AFPM machine was driven by a d.c. motor (at no load) and allowed to operate as a conventional fan as shown in Figure 7. The machine was set up with a discharge duct. Along one side of the duct, several tapping points were made for measuring the static pressure with a Manometer. Near the outlet of the duct provision was made whereby the velocity is measured using a hot-wire anemometer probe.

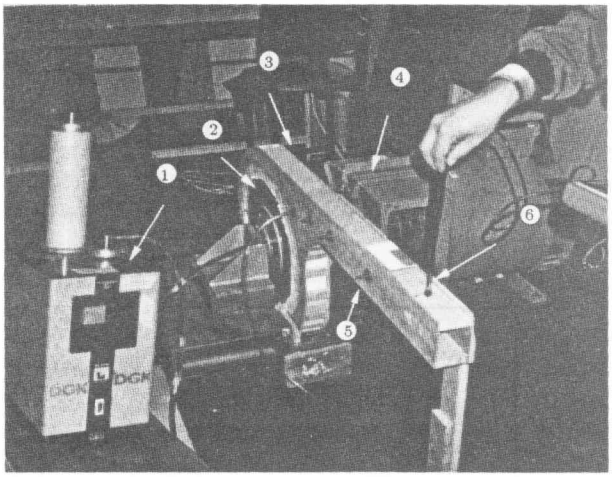

Figure 7 The experimental set-up, where 1 - manometer, 2 - AFPM machine, 3 - discharge duct, 4 - drive machine, 5 - pressure tapping point, 6 - hot-wire anemometer probe

The static pressure difference Δp was measured as a function of volumetric flow rate $Q = A$ v for different motor speeds varying from 200 to 1400 r.p.m. The results are plotted in Figure 8. Note that the pressure losses occurring in the discharge duct have been subtracted from the measured values.

Volumetric flow rate

Figure 9 shows both the computed and measured volumetric flow rate of the AFPM machine (Figure 1) at different operating speeds. It can be seen that the correlation between the computed and measured results is good. This confirms that shock and leakage losses, as previously assumed, become less significant as the operating point is approached.

Thermal model

Lumped-parameter circuits, consisting of a network of thermal resistances, nodal temperatures and heat sources, have been widely used to represent the complex distributed thermal parameters of electrical machines.[1,12]

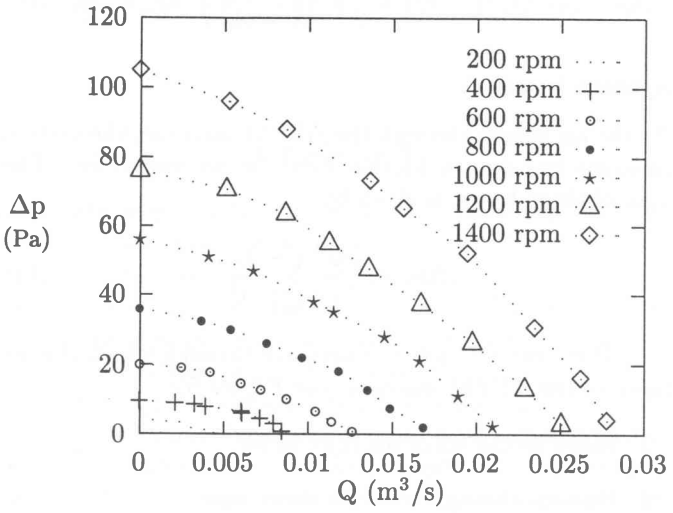

Figure 8 Measured characteristic curves of pressure against flow rate for the AFPM machine ($\rho = 1.177$ kg/m^3)

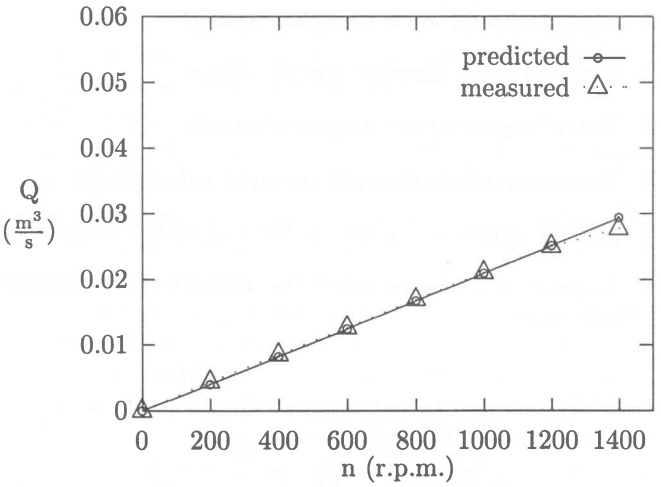

Figure 9 Calculated and measured volumetric flow rate as a function of speed

Thermal resistance circuit

Figure 10(a) shows a sectional view of an AFPM machine. It can be observed that the AFPM stator is symmetrical from a heat transfer perspective. It is therefore reasonable to model only half of the machine (see Figure 10(b)).

The heat flowing through each path of the thermal resistance circuit is given by a temperature difference divided by a thermal resistance (Table 1). The net heat transfer for radiation between two surfaces may be given by[10]

$$\dot{Q} = \frac{\sigma\left(T_2^4 - T_1^4\right)}{\frac{1-\epsilon_1}{\epsilon_1 A_1} + \frac{1}{F_{12} A_1} + \frac{1-\epsilon_2}{\epsilon_2 A_2}} \qquad (13)$$

In this equation it is seen that the heat transfer depends on the difference of the fourth power of the absolute

temperature, surface spectral property ϵ and surface orientation taken into account by a form factor F. Convective heat transfer from a surface to a moving fluid depends on the heat transfer coefficient, the determination of which is a complex problem, usually necessitating the use of empirically determined correlations. No convection heat transfer correlations relating to the specific topology of AFPM machines are available and for this reason potentially suitable existing correlations are dealt with in the next section.

Convection heat transfer coefficients

The rotating disc system plays a major role for the cooling and ventilation of the AFPM machine. Accurately determining the convection heat transfer coefficients needs thorough theoretical and experimental investigation because of the complexity of the flow regimes. In this section the convection heat transfer coefficients in different parts of the AFPM machine are evaluated exploiting a number of existing models.

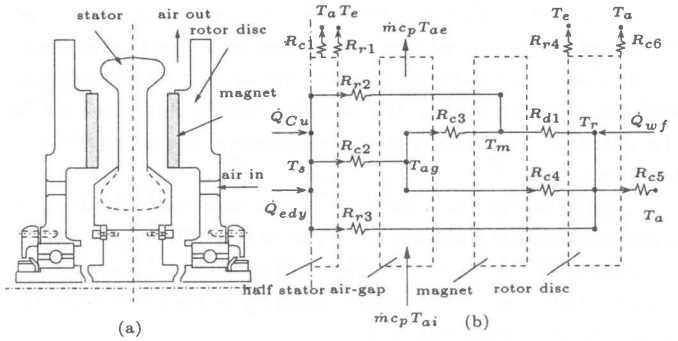

Figure 10 The thermal resistance circuit of an AFPM generator

Table 1 Definition of the thermal resistances in Figure 10(b)

Symbols	Definition
R_{c1}	Convection: stator end-winding to air
R_{c2}	Convection: stator to air-gap
R_{c3}	Convection: air-gap to magnets
R_{c4}	Convection: air-gap to rotor disc
R_{c5}	Convection: rotor disc to open air
R_{c6}	Convection: rotor periphery to air
R_{r1}	Radiation: end winding to open air
R_{c1}	Radiation: stator to magnets
R_{r2}	Radiation: stator to rotor disc
R_{r3}	Radiation: stator to rotor disc
R_{r4}	Radiation: rotor periphery to air
R_{d1}	Conduction: magnets to rotor disc

Free rotating disc

The average heat transfer coefficient at the outside surface of a rotating disc may be evaluated using the formulae developed for free rotating plate,[14], i.e.

$$\bar{h} = \frac{k}{R} \cdot \overline{Nu} \tag{14}$$

where $\overline{Nu}$ is given according to different flow conditions as follows:

(i) For combined effects of free convection and rotation in laminar flow (Figure 11(a))[14]

$$\overline{Nu} = \frac{2}{5} \cdot \left(\mathrm{Re}^2 + Gr\right)^{\frac{1}{4}} \tag{15}$$

where $\mathrm{Re} = \dfrac{\omega R^2}{\upsilon}$, $Gr = \dfrac{\beta g R^3 \pi^{\frac{3}{2}} \Delta T}{\upsilon^2}$ and ΔT is the temperature difference between the disc surface and the surrounding air.

(ii) For a combination of laminar and turbulent flow with the transition at $r_c = \left(2.5 \times 10^5 \upsilon/\omega\right)^{1/2}$ (Figure 11(b))[14]

$$\overline{Nu} = 0.015 \cdot \mathrm{Re}^{0.8} - 100 \cdot \left(\frac{r_c}{R}\right)^2 \tag{16}$$

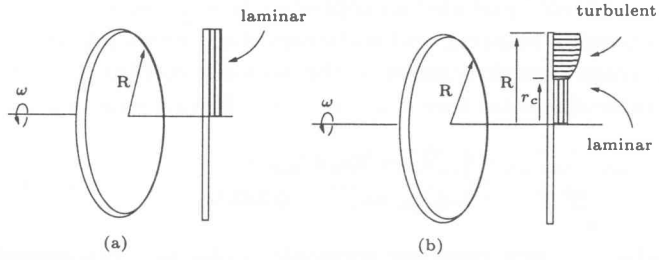

Figure 11: Free rotating disc, where (a) laminar flow, (b) laminar and turbulent flow

It is instructive to compare the heat transfer capabilities between a rotation disc and a still-standing disc. Considering the AFPM machine depicted in Figure 1, which has a diameter of 0.4 m and rotates at 1 260 r.p.m., the convection heat transfer coefficient may be calculated as 41 W/m^2 K, which is about ten times that of the same disc at standstill. Alternatively, one can say that the effective heat dissipation area of the same disc can be increased by a factor of 10 when rotating.

Rotor edge

The heat transfer correlations for the radial periphery of the rotor disc is similar to that of a rotating cylinder in air. In this case the average heat transfer coefficient is given as

$$\bar{h}_p = (k/D)\,\overline{Nu} \tag{17}$$

where $\overline{Nu} = 0.133 \cdot \mathrm{Re}_D^{2/3}\,\mathrm{Pr}^{1/3}$, D is the diameter of the cylinder and $\mathrm{Re}_D = \omega D^2/\nu$. When using Equations (15), (16), and (17), a uniform temperature distribution in the cylinder is normally assumed. Applying these equations to the rotor disc, the average heat transfer coefficient around the radial periphery is found to be about 95 W/m^2 K which therefore justifies its presence in the thermal resistance circuit. Since h_p is proportional to the rotational speed ω, it may be concluded that the rotor periphery plays an increasingly important role in the heat dissipation as ω increases.

Rotor-stator system

As seen in Figure 1, the main heat transfer region consists of surface-mounted PMs with radial channels between the PMs. Due to centrifugal effects, there is a forced flow through the PM channels, which increases the local heat transfer rate compared to that of a free disc. The relative increase will depend on the gap ratio, $G = \frac{s}{r_o}$, the mass flow rate and the rotational speed of the system under consideration.[15]

Having radial channels and thick impellers, an air-cooled AFPM machine may be regarded as a poorly designed fan from a fluid flow perspective. Its tangential velocity component is much larger than the radial component. Thus, the heat transfer rate near the rotating disc shows more dependence on the rotational Reynolds number, which is defined as[16]

$$\mathrm{Re} = \rho\omega^2 r_o/\mu \tag{18}$$

Owen[17] provided an approximate solution for the flow between a rotating and stationary disc, which relates the average Nusselt number to the moment coefficient of the stator-side rotor face, C_{mo}, by the following equation.

$$\begin{cases} \overline{Nu} = \mathrm{Re}_r\, C_{mo}/\pi \\ C_{mo}\,\mathrm{Re}_r^{1/5} = 0.333\lambda_T \end{cases} \tag{19}$$

where λ_T is a *turbulent parameter* given as a function of volumetric flow rate, Q, as follows

$$\lambda_T = \frac{Q}{\nu r_o}\,\mathrm{Re}_r^{-\frac{4}{5}} \tag{20}$$

Applying Owen's approximate solution[17] to the same AFPM machine operating at a speed of 1 260 r.p.m. with a measured radial flow of 0.026 m^3/s between rotor and stator, the estimated average heat transfer coefficient from the stator across the air-gap to the rotating disc is 94 W/m^2 K. As discussed in Owen,[16] it has been shown that for a small gap ratio ($G < 0.1$) the flow in the air-gap space between the rotor and stator can be treated as a boundary layer. Whilst it is not necessarily true that the convective heat transfer coefficient from the stator to the air flow is close to that from the air flow to the rotating disc, the same heat transfer coefficient has been assumed in the thermal circuit simulation.

Conservation of energy

Applying the conservation of energy, the rate of internal energy change of a control volume may be written as follows:

$$\frac{\Delta U}{\Delta t} = \dot{Q}_{in} - \dot{Q}_{out} + \dot{m}_{in}i_{in} - \dot{m}_{out}i_{out} \tag{21}$$

For steady-state conditions, $\frac{\Delta U}{\Delta t} = 0$ and therefore,

$$0 = \dot{Q}_{in} - \dot{Q}_{out} + \dot{m}_{in}i_{in} - \dot{m}_{out}i_{out} \tag{22}$$

Equation 22 is applied to each part (the half-stator, air-gap, magnet, and rotor disc) of the AFPM machine shown in Figure 10 to obtain a set of equations with the temperatures of the parts being the only unknowns. The heat flowing in each path is given as a temperature difference divided by a thermal resistance. The values used for the heat source terms are given in Table 4.[19] This set of equations are rather complex but is readily solved using *Gauss-Seidel* iteration, for example.

Temperature measurements

The AFPM machine is driven by a d.c. motor as shown in Figure 7 and operates as a generator feeding a rectifier load. Both rated and overload (double the rated current) operating conditions are monitored. The temperature of the rotating disc and the peripheral edge of the windings are measured using a digital infrared thermometer.

The average winding temperature was measured using an electrical resistance method.[12] The machine was run for a long enough time to ensure steady-state conditions. The driving motor was then shut down and when the machine came to standstill the electrical resistances of the three phases of the windings were measured as a function of time. A suitable curve is fitted to these resistance measurements and the resistance that the winding would have had when the machine was shut down is determined by extrapolating back in time.

For ensuring the validity of the measurements the first resistance reading should be taken within 30 seconds after switching off the power to the driving motor. The average temperature rise in the stator winding is then obtained by using the following equation:

$$\Delta T = \frac{R_2 - R_1}{R_1}(K + T_1) + T_1 - T_0 \tag{23}$$

where K is a constant ($K = 235$ for copper winding, $K = 228$ for aluminum winding), T_0 is the ambient temperature, T_1 is the cold winding temperature, R_1 and R_2 are the cold and hot winding resistances.

Comparison of results

The computed values of the temperature rise in the various parts of the AFPM machine are compared with the corresponding measurements in Tables 2 and 3. It is evident that the predicted temperature values are somewhat higher than that of the measurements. The calculated results agree reasonably well with the tested results, considering the relatively simple thermal resistance network used to represent the AFPM machine.

Discussion and conclusions

The main aim of this study has been the development and verification of a thermo-fluid model for analyzing and predicting thermal behavior of AFPM machines.

Table 2 Predicted and measured temperature rises (T_{amb} = 23.75°C, I_{ph} = 30 A, n = 1 217 r.p.m.)

Machine parts	Calculated (°C)	Measured (°C)
Stator winding	27.8	23.3
Rotor disc	14.1	11.2
Rare-earth PM	13.7	–
End winding	–	21.5
Air-gap	7.6	–

Table 3 Predicted and measured temperature rises (T_{amb} = 24°C, I_{ph} = 60 A, n = 1 263 r.p.m.)

Machine parts	Calculated (°C)	Measured (°C)
Stator winding	102.1	95.1
Rotor disc	27.3	25.5
Rare-earth PM	27.6	–
End winding	–	65.4
Air-gap	30.1	–

Table 4 Heat source terms for the AFPM machine[19]

Description	Q
Bearing frictional losses	106 W
Stator eddy current losses	23 W
Magnet eddy current losses	3 W
Stator copper losses	360 W
Stator copper losses (overload)	1 440 W

The comparison between the calculated results and the measurements has shown that the developed model can perform the thermal analysis with reasonable accuracy. The predicted temperature values are invariably higher than the measured ones. One possible reason is that the endwinding is partially located above the PM top edge and its heat flow path is not necessarily through PMs. Including end-winding losses as internal heat losses may result in slightly over-estimated temperature values in the analysis.

It should be noted that the determination of the air temperature in the air-gap is only possible if the mass flow rate through the air-gap can be somehow predicted, hence the necessity of a reasonable fluid-flow model.

The fluid flow model gives reasonable results, however it may be somewhat limited because the effect of rotation in the system losses as given in Eqn. 11 was neglected.

The air flow through the AFPM machine is not optimized from a minimum energy loss point of view. This is evident by the tortuous path through which the air flows. By taking into account to a greater degree sound fluid mechanics practice, an improved mass flow rate could be achieved with a subsequent reduction in the operating temperature and hence a longer service life.

Planned future work includes applying the revised thermofluid model to a double-stage AFPM machine. Comparison will be done to further check the validity of the model. The ultimate goal is to realize the fast temperature prediction of general AFPM machine with reasonable accuracy at design stage.

Acknowledgements

This paper was supported by the University of Stellenbosch. RW wishes to thank A Swart, CJ Zietsman and DN Mbidi for their assistance in the assembling of the testing equipment.

References

1. E Spooner & BJ Chalmers. TORUS: a slotless, toroidal-stator, permanent-magnet generator. *Proceedings of IEE*, **139**, pp.497–506, 1992.
2. CC Chan. Axial-field Electrical Machines with Yokeless Armature Core. PhD thesis, University of Hong Kong, 1982.
3. JF Gieras & M Wing. *Permanent Magnet Motor Technology: design and applications.* Marcel Dekker, NY, 1997.
4. JF Douglas, JM Gasiorek & JA Swaffield. *Fluid Mechanics.* Longman, UK, 1995.
5. AT Sayers. *Hydraulic and Compressible Flow Turbomachines.* McGraw-Hill, UK, 1990.
6. FM White *et al. Fluid Mechanics.* McGraw-Hill, NY, 1994.
7. BR Munson, DF Young & TH Okiishi. *Fundamentals of Fluid Mechanics.* Wiley, NY, 1994.
8. D Chisholm. *Two-phase flow in pipelines and heat exchangers.* George Godwin, NY, 1983.
9. DS Miller. *Internal Flow Systems.* BHRA (Information Services), UK, 1990.
10. AF Mills. *Basic Heat and Mass Transfer.* Irwin,1995.
11. PJ Strachan, PP Reynaud & TW von Backström. The Hydrodynamic Modeling of Torque Converters. *R & D Journal*, **8**, pp.21–29, 1992.
12. RH Engelmann & WH Middendorf (ed.). *Handbook of Electric Motors.* Marcel Dekker, NY, 1995.
13. DE Metzger & NH Afgan (ed.). *Heat and Mass Transfer in Rotating Machinery.* Hemisphere, Washington, 1984.
14. WY Wong. *Heat Transfer for Engineers.* Longmans, 1977.
15. JM Owen. The Effect of Forced Flow on Heat Transfer From a Disc Rotating Near a Stator. *International Journal of Heat and Mass Transfer*, **14**, pp.1135–1147, 1971.

16. JM Owen. The Reynolds Analogy Applied to Flow Between a Rotating and a Stationary Disc. *International Journal of Heat and Mass Transfer.* **14**, pp.451–460, 1971.

17. JM Owen. An Approximate Solution for the Flow Between a Rotating and a Stationary Disk. *ASME Journal of Turbomachinery*, **111**, pp.323–332, 1989.

18. JM Owen & RH Rogers. *Flow and Heat Transfer in Rotating-Disc Systems*, **1**. Research Studies Press Ltd, UK, 1989.

19. NF Lombard & MJ Kamper. Analysis and Performance of an Ironless Stator Axial Flux Permanent Magnet Machine. *IEEE Trans. Energy Conversion*, **14**, pp.1051–1056, 1999.